Pressure radiation from a perforated duct exit region

Wang, Honglin; Vardy, Alan, E; Pokrajac, Dubravka

Published in:
Journal of Sound and Vibration

DOI:
10.1016/j.jsv.2015.03.040

Publication date:
2015

Document Version
Peer reviewed version

Pressure radiation from a perforated duct exit region

Wang, Honglin; Vardy, Alan; Pokrajac, Dubravka

Published in:
Journal of Sound and Vibration

DOI:
10.1016/j.jsv.2015.03.040

Publication date:
2015

Pressure radiation from a perforated duct exit region

Honglin Wang [1], Alan E Vardy [2], Dubravka Pokrajac [3]

[1] School of Mechanical Engineering, Southwest Jiaotong University, China
[2] Civil Engineering Division, University of Dundee, UK
[3] School of Engineering, University of Aberdeen, UK

Corresponding author:
Alan VARDY, Research Professor

Address for correspondence:
Dundee Tunnel Research, Kirkton, Abernyte, Perthshire, PH14 9SS, Scotland
E: a.e.vardy@dundee.ac.uk
T: +44 (0) 1828 686 241

Abstract: *The influence of a perforated extension region on pressures radiated from the end of a duct is studied numerically using CFD. Planar 2D geometry is considered and particular attention is paid to the case of pressure disturbances radiated from railway tunnels in cut-and-cover regions. The mechanism that causes this behaviour is described and it is shown to have an important influence of the effectiveness of a perforated extension region. It is found that such regions can strongly reduce the pressures radiated from a duct outlet, but that this benefit is offset by pressures radiated directly from the holes along the perforated region itself. In the particular case of tunnel design, practical studies of wave transmission are usually based on 1-D, plane-wave, analyses. Accordingly, attention is paid to assessing the limitations of such approaches in the case of wave propagation along a perforated region.*

Keywords: *wave reflection, wave transmission, perforated duct, micro-pressure wave, tunnel extension, counter-measures, sonic boom.*

List of Symbols

e	total energy per unit mass of air [J/m^3]
F,G	defined in Eq.(1)
H_{tun}	internal height of tunnel [m]
H_{slot}	roof thickness [m]
L_1	length of main tunnel upstream of perforated region [m]
L_{tun}	length of tunnel plus perforated extension [m]
MPW	micro-pressure wave
p	absolute pressure [Pa]
$(\partial p/\partial t)_0$	steepness of principal incident wavefront [Pa/s]
R_{gas}	gas constant [J/kg.K]
R	distance between MPW reference line and nearest part of tunnel [m]
T	absolute temperature [K]
t	time coordinate [s]
U	defined in Eq.(1)
u,v	velocity components in x,y directions [m/s]
W_{slot}	width of roof slot [m]
X_{slot}	distance between slot centres [m]
x	axial coordinate [m]
y	lateral coordinate m]

Greek characters

ρ	air density [kg/m^3]
γ	ratio of principal specific heat capacities [-]

1 Introduction

When a pressure wave travelling along a duct reaches an open outlet end, the principal consequence is reflection process that causes a new wave to propagate back along the duct. Another consequence is a change in the rate of mass flow to/from the duct from/to the external environment and this inevitably induces pressure changes in the external flow field. Usually, this is of little importance to persons studying the internal wave propagation and, often, it is also of little consequence externally. Occasionally, however, especially in the case of the reflection of steep-fronted waves, the resulting external disturbances can be undesirably large. Examples include vehicle exhaust systems, firearms and tunnels used by high-speed trains. In such cases, designers need to provide suitable remedial measures and many possible generic options can be considered. The particular choice of remedial measure depends strongly on the application as well as upon the flow regime. For example, whereas an exhaust muffler can often be hidden beneath a vehicle, a similar geometry at the end of a railway tunnel would rarely be visually acceptable. This paper focuses on the particular case of a railway tunnel portal at the end of a cut-and-cover region.

Aerodynamic disturbances caused by trains travelling through tunnels give rise to several phenomena that need to be considered by designers and operators of the tunnels [1]. The phenomena are typically quite small (e.g. pressure fluctuations rarely exceed 5% of an atmosphere even with very high speed trains) but the potential consequences can be of high importance. For instance, strong air velocities require robust fixings for all equipment and sudden pressure changes require trains to be sealed to ensure adequate passenger comfort [2,3]. In certain circumstances, disturbances inside a tunnel can give rise to related disturbances outside tunnels – e.g. turbulence-generated noise from high velocities in airshafts [4]. A special problem that has received a great deal of attention in recent decades is the emission of so-called micro-pressure waves (MPWs) from tunnel portals into the surrounding environment [5]. Such waves always occur when internal pressure waves reflect at a tunnel portal, but their amplitudes are usually far below the limits of acceptability. The most commonly cited exception occurs when a high speed train enters a slab-track tunnel of moderate length. In such cases, the pressure wave generated by nose-entry steepens as it propagates along the tunnel and can become almost a shock wave before reaching the exit portal. If no countermeasures were in place, this could give rise to a strong audible sound (sonic boom) outside the tunnel as well as to high amplitude infra-sound that could shake adjacent buildings. Such behaviour was first encountered during commissioning of the earliest high-speed railways in Japan [6].

The most common counter-measure to prevent the occurrence of unacceptable MPWs is the building of special *entrance* regions for tunnels [7,8,9]. The purpose of these is to elongate the nose-entry wavefront sufficiently to ensure that, even after steepening during propagation along the tunnel, it is not too steep when it reaches the exit portal. This has proved to be a highly effective counter-measure, but it has some important limitations. First, the required length of the modified entrance region typically increases approximately with the cube of the train speed. Second, the required length increases with the length of the tunnel. Third, entrance region counter-measures have no influence at all on wavefronts that are generated further along the tunnel, notably when a train crosses an airshaft or other branch feature in a tunnel. When these limitations are relevant, it is logical to consider counter-measures further along the tunnel. One possibility that has been considered, but found to be less effective than expected is the provision of baffle plates along a tunnel [10]. Greater success has been obtained with measures that can be applied at outlets from which unacceptable disturbances must be prevented. This paper focuses on the most important of these locations, namely the main tunnel *exit* portal.

Several exit portal countermeasures have been studied. Passive methods include chambers that are loosely analogous to gun-silencers or automobile exhaust silencer boxes [11,12]. Typically, these include some form of baffle plates, possibly in a helical formation [13]. However, all such devices have a fundamental disadvantage of requiring a large structure in the affected region – which is contrary to the usual wishes of designers to minimise the visual impact of tunnels. This particular disadvantage can be avoided by employing active measures to generate so-called anti-noise, namely a second set of MPWs that, ideally, is equal to the train-generated MPWs, but opposite in sign [12,14,15]. An obvious disadvantage of such techniques – apart from the technical difficulties involved in their design – is that they are not fail-safe. That is, in the event of a power failure, they would provide no relief at all and, in the event of malfunction, they could even increase the disturbance.

In this paper, attention is focussed on a tunnel exit counter-measure comprising an extended region of tunnel with holes/slots along its length leading directly to the atmosphere (Fig-1a). This is geometrically similar to one form of existing tunnel *entrance* regions (which automatically become exit regions when the direction of train travel is reversed). In a nutshell, the objective is to cause the incident wavefront to elongate as it propagates along the extension, thereby greatly reducing its steepness and hence reducing the MPW emission through the final outlet portal. However, there is a price to pay for this, namely the creation of additional MPWs from the slots along the tunnel roof. The latter have been assessed in an experimental and numerical investigation of a related geometry, namely snow sheds between adjacent tunnels in a mountainous region of Japan [16].

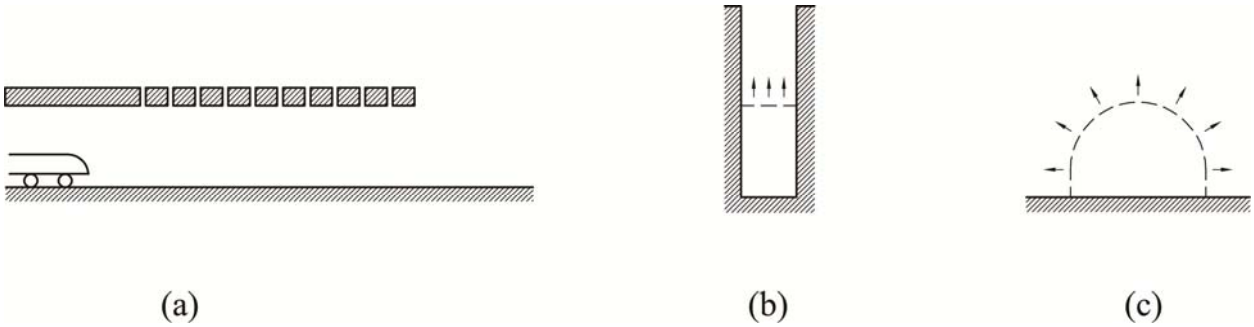

Fig-1 Indicative geometries of perforated exit regions
(a) Longitudinal elevation
(b) Cut and cover portal region (this paper)
(c) Overland portal region

Before studying the flow in detail, it is useful to explain why extended exit regions have not always been preferred to extended *entrance* regions. There are two main reasons. First, the maximum effective elongation of a nose-entry wavefront by an entrance region is strongly influenced by the (relatively large) time needed for a train to travel the length of the entrance region. For all train speeds below a Mach number of 0.5, when the train nose reaches the end of the region, the toe of the nose-entry wavefront is further ahead of the train than the length of the region itself. The total elongation exceeds the entrance length by the proportion $(1/M_z - 1)$, where M_z denote the train Mach number. In contrast, the maximum effective elongation of a wavefront at an *exit* region is only the length of the region itself. Second, the most important design parameter for an entrance region is the design train speed (which will usually be known with good accuracy) whereas, as shown below, the key parameter for an exit region is the steepness of the incident wavefront (which will rarely be known with good accuracy).

Although the use of extended exit regions has not been studied extensively, some attention has been paid to them [e.g. 17,18,19]. In most such studies, the principal interest has been on the influence of the regions on the reflection of waves *inside* tunnels, with special reference to passenger pressure comfort on board trains. One important conclusion of such work is that *perforated* exit regions are potentially far more advantageous than *flared* exit regions for such purposes. It is fortunate that the same conclusion also pertains to the influences of the two types of exit region on acoustic radiation from tunnels.

Figure-1(b &c) shows two possible geometries for tunnel portal regions. One, indicative of a tunnel emerging into a cut-and-cover region, might sometimes be incorporated rather easily into a tunnel design simply by adjusting the roof configuration. The other, indicative of a tunnel emerging into a region of open ground, might be less easy to create without some visual disturbance. The cut-and-cover configuration approximates to a planar 2-D geometry whereas the more open configuration approximates more closely to axi-symmetric geometry. Broadly similar behaviour may be expected in the two cases, but there are some differences because waves expanding in the constrained environment of a cut-and-cover geometry cannot attenuate as rapidly as those in a more open environment. Herein, attention is focussed on the planar 2-D case.

In a cutting such as that depicted in Fig-1(b), the early part of the response of a wave after reaching a slot in the tunnel roof will be dictated by 2-D geometry, but later parts of the response will be increasingly influenced by the 3-D environment above the cutting. The use of 2-D analysis in this paper therefore implies a focus on small times. The analysis is directly applicable until wave reflections begin to arrive from the 3-D region and it becomes increasingly less representative thereafter. There are two reasons for accepting this limitation. First, the wave propagation *inside* the tunnel is more sensitive to short-time influences of reflections from the roof slots than to long-time ones – and this is also true of the largest pressure fluctuations inside the cutting. Second, the most obvious alternative to planar 2-D geometry would be axi-symmetric 2-D geometry which is more representative of cases such as that depicted in Fig-1(c). Strictly, neither of these 2-D approximations is valid in the case of real tunnels because 3-D features always exist. However, the additional detail obtainable from a fully 3-D CFD analysis will rarely justify the large additional increase in computer power that it would necessitate except, perhaps, in specific practical applications.

The overall purpose of this paper is to assess the influence of perforated exit regions on (i) MPWs radiated outside the tunnel (from the slots as well as from the main portal) and on (ii) reflected waves along the main tunnel itself. The theoretical approach presented in Section 2 is first applied to a base-case geometry with no roof slots. For practical purposes, this may be regarded as the scenario that needs to be alleviated by the modified exit region. The influence of a perforated region on both internal and external pressures is then considered, and the dependence on the steepness of the incident wavefront is assessed. In addition to drawing general conclusions from the work, the opportunity is taken to assess briefly the capability of 1-D methods to model the reflection process inside the tunnel.

2 Numerical study

At a detailed level, unsteady flows generated by trains travelling inside railway tunnels are compressible, three-dimensional and turbulent in nature. However, unsteady phenomena that are significantly longer than the tunnel hydraulic diameter can be modelled with good accuracy by 1-D

methods that use plane wave approximations to represent the propagation of pressure disturbances. The large-scale behaviour of the flow in a train–tunnel system is typically analysed in this way [20,21,22,23,24] and the cumulative influence of discrete, localised regions of strongly 3-D flow is allowed for by means of empirical coefficients of stagnation pressure loss. Important examples of such regions are those close to the ends of a train and in the wake region behind it. A 1-D approach to analysis is especially suitable for general engineering design (i) because of its relatively small demands for computational resources, (ii) because it avoids the need for detailed geometrical input and (iii) because the outcomes are easily interpreted.

Notwithstanding these advantages, quasi 1-D models are wholly incapable of capturing inherently 2-D or 3-D features of the flow and hence they are not suitable for studying crucially important aspects of the flows under consideration herein. Consider the flow depicted in Fig-2(a) & (b), for instance, where a plane wave front reflects at a tunnel exit portal. To highlight the underlying behaviour, the special case of a plane shock wavefront is depicted. The whole of the wavefront arrives at the exit plane at the same instant. Up to this point, the behaviour is independent of the vertical position within the tunnel cross-section. In the next few moments, it depends markedly on the particular location. At the roof, the flow is immediately influenced by the freedom to expand laterally as well as axially whereas, at the floor of the tunnel, it is initially uninfluenced by the external environment. It remains uninfluenced until it is affected by the waves depicted expanding radially from the roof. These do not reach the floor until after an interval of H_{tun}/c, where H_{tun} denotes the tunnel height and c is the local speed of sound. At that time, the lower part of the wavefront has already moved axially by a distance H_{tun} from the portal plane. In real tunnels, the incident wavefronts are not true shock waves, but this description is nevertheless indicative of the main process leading to the emission of MPWs from a tunnel.

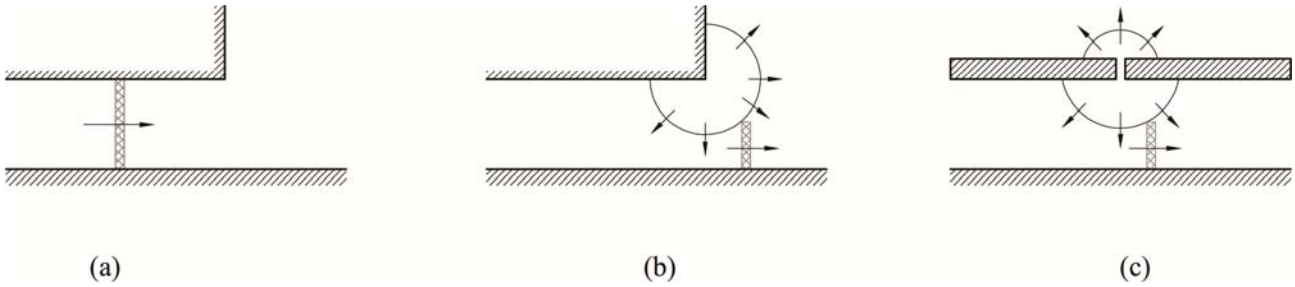

Fig-2 Indicative influence of 2-D/3-D geometry on plane wave propagation
(a) Plane wave approaching an exit portal
(b) Reflection and transmission at an exit portal
(c) Reflection and transmission at a roof slot

Broadly similar effects occur whenever a wave propagating along a perforated extension region meets a hole in the tunnel roof - see Fig-2(c). As a consequence, it is not possible for a wavefront to propagate along such a region in the manner of a plane wave. Instead, strong differences must be expected between the behaviour close to the perforated roof and the corresponding behaviour some distance away from it. This will further distort the behaviour of MPWs radiating from the portal plane. Furthermore, MPWs radiating from individual slots will be influenced by cross-sectional pressure variations as well as by axial variations. Accordingly, it is necessary to use an analysis that allows for at least 2-D behaviour. For complete coverage of all effects, a full 3-D analysis would be required, but the most important features of the flow can be captured using 2-D methods. In particular, the most important consequences of the freedom for waves to expand laterally will be well approximated by 2-D methods. Further modulations due to phenomena that

are inherently fully 3-D will have weaker consequences, at least for the overall wave propagation along the tunnel.

2.1 Governing equations

The propagation of wavefronts along short lengths of tunnel approximates closely to inviscid flow, primarily because the Reynolds numbers are large (typically in excess of 10^6). Accordingly, the unsteady flow can be simulated with good accuracy using the Euler equations, which, for planar 2_D geometry, may be expressed as [25]:

$$\frac{\partial \mathbf{U}}{\partial t}+\frac{\partial \mathbf{F}}{\partial x}+\frac{\partial \mathbf{G}}{\partial \mathrm{y}}=0 \tag{1}$$

where,

$$\mathbf{U}=\begin{bmatrix}\rho\\ \rho u\\ \rho v\\ \rho e\end{bmatrix} \qquad \mathbf{F}=\begin{bmatrix}\rho u\\ \rho u^2+p\\ \rho uv\\ (\rho e+p)u\end{bmatrix} \qquad \mathbf{G}=\begin{bmatrix}\rho v\\ \rho uv\\ \rho v^2+p\\ (\rho e+p)v\end{bmatrix}$$

in which x and y are axial and lateral coordinates, t is the time coordinate, u and v are velocity components in the x and y directions, and ρ and p are the air density and absolute pressure. The total energy per unit mass of air, e, is the sum of the kinetic and internal energies, namely:

$$e=\frac{p}{\rho(\gamma-1)}+\frac{u^2+v^2}{2} \tag{2}$$

in which γ denotes the ratio of the principal specific heat capacities of the air. The equations are closed by regarding the air as a perfect gas satisfying the equation of state:

$$p=\rho R_{gas}T \tag{3}$$

where R_{gas} is the gas constant for air and T is the absolute temperature.

2.2 Solution domain, boundary conditions and initial conditions

The geometry of the simulation domain is shown in Fig-3. It includes the end region of tunnel upstream of the perforated exit region and it extends laterally and axially outside the tunnel sufficiently far to ensure that the remote boundary to have negligible influence during the period of study. That is, the time taken for waves to propagate from the tunnel to the boundary and back again exceeds the time for which results are studied.

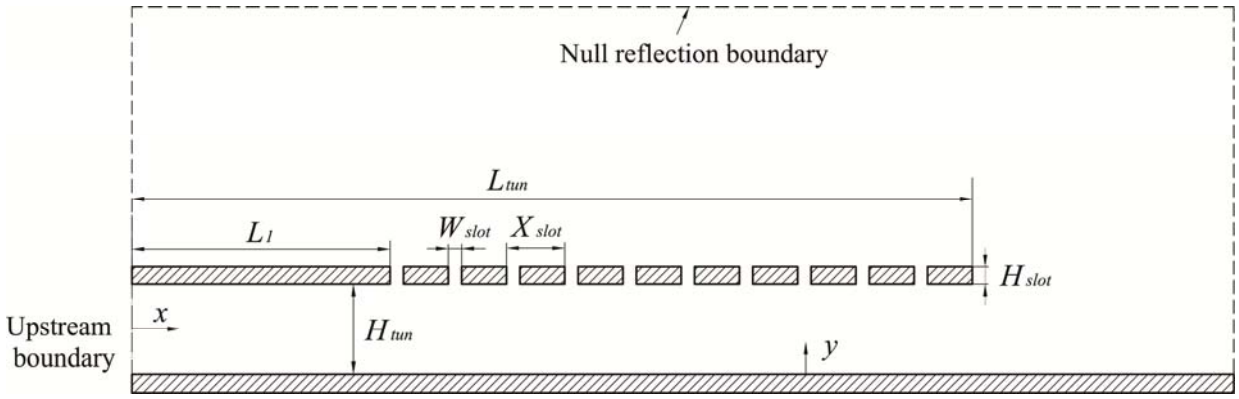

Fig-3 Tunnel geometry and simulation domain

A free-slip condition is applied along all solid surfaces and a null-reflection condition is applied on all other external boundaries. These boundaries are located sufficiently far from the tunnel to ensure that they do not influence the results presented below. This is necessary because it is not possible to achieve wholly non-reflecting conditions when waves propagate in a 2-D or 3-D manner. At the upstream boundary inside the tunnel, the pressure is prescribed to increase linearly from t = 0 and then to be constant. This is loosely representative of a typical train-generated wavefront and it is sufficiently simple to avoid the risk of obtaining outcomes dependent upon non-linearities that distinguish particular wavefront shapes in specific tunnels (or other applications). The temperature at this boundary is prescribed to vary isentropically with the prescribed pressure.

The initial condition is uniform pressure and zero velocity over the whole domain. All subsequent variations of pressure and velocity arise solely as a consequence of the pressure wavefront caused by the varying pressure at the upstream boundary.

The overall simulation domain extends from (x,y) = (0,0) to (320,109). The length of the perforated region of duct (tunnel) is 100 m and the distance from the upstream boundary is L_1 = 120 m so the portal plane is at x = 220 m. There are ten slots of width W_{slot} = 0.8 m at intervals of X_{slot} = 10 m. The tunnel height is H_{tun} = 8 m and its roof thickness is H_{slot} = 1.0 m. The upstream boundary is not intended to represent a physical boundary. It is simply a location that is sufficiently far upstream for the pressure history to be prescribed independently.

2.3 Solution method and validation

Many well known software packages are capable of solving the Euler equations accurately provided that they are used correctly. The particular software used herein is ANSYS FLUENT [26] and the spatial numerical grid is as shown in Fig-4. The options chosen in FLUENT are density-based solver, Roe-FDS Flux Scheme, third-Order MUSCL for spatial discretization and 2nd-order implicit time stepping for temporal discretization.

For simulations presented herein, a grid size of $H_{tun}/80$ = 0.1 m is used over the whole of the solution domain inside the tunnel and close to the tunnel. An increased grid size is used in the far field where pressure wave amplitudes are much smaller than in the near field and where rates of change are even smaller. The chosen grid would be too coarse to reproduce detailed *flow* structures close to the corners of the slots (indeed, no grid could achieve this exactly for the assumed inviscid flow), but it is more than adequate for simulating *wave* propagation through the slots. This is because the time scales associated with wave propagation across the slots are small

in comparison with scales of practical relevance to the resulting MPWs. The adequacy of the numerical methodology is now confirmed in a more formal manner by means of two examples that exhibit strong wave behaviour.

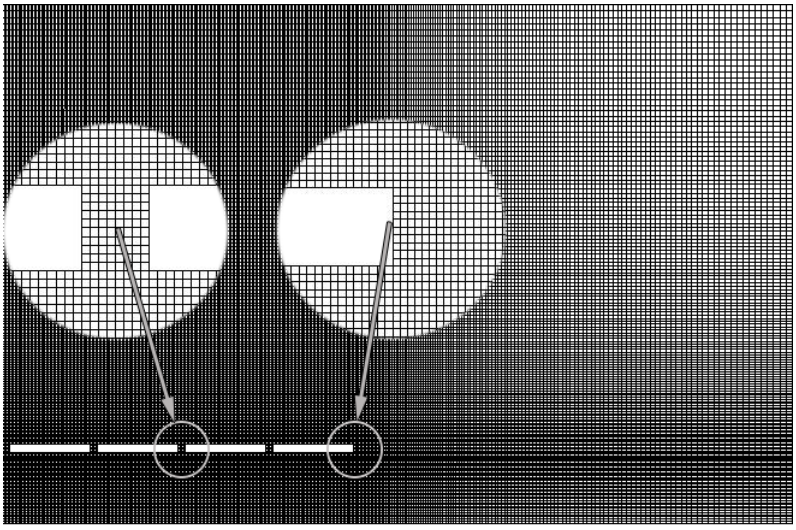

Fig-4 Numerical grid structure

Figure 5 depicts a steep wavefront propagating along a uniform duct. Although the Mach number in the region of fastest flow is very small (less than 0.014), the rate of change of pressure at the wavefront is so great that the steepening process is the dominant visual feature of the Figure. This wavefront is much steeper than would be acceptable in practical tunnel operation so this is a highly demanding test of the CFD methodology. The figure shows pressure profiles at five instants. The first is 0.1 s after the toe of the wavefront is initiated at the upstream boundary and the others are at successive intervals of 0.5 s.

The broken lines show the CFD predictions and the continuous lines depict a quasi-analytical solution obtained in a step-wise manner based on plane-wave behaviour (uniform conditions over each cross-section). At any point in (x,t) space, the local wave speed is the sum of the local particle speed U and the local speed of sound c. Thus the tip of the wavefront propagates at the speed of sound of the undisturbed flow and all other parts propagate at greater speeds (U+c). Using the CFD velocity distribution $U\{x\}$ at t = 0.1 s as an initial condition, the sound speed distribution is deduced from the isentropic wave propagation equation:

$$\frac{2}{\gamma - 1}(c - c_{0.1s}) - (U - U_{0.1s}) = 0 \qquad (4)$$

The slight curvature of the continuous lines arises because the axial distribution of velocity at t = 0.1 s is not quite linear (NB: the prescribed upstream boundary condition, namely constant $\partial p/\partial t$, does not imply uniform $\partial p/\partial x$ or uniform $\partial U/\partial x$).

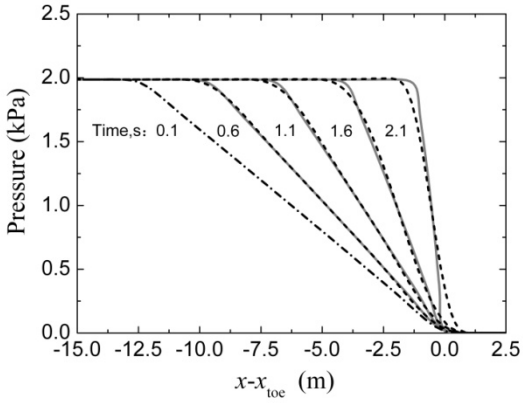

Fig-5 Assessment of numerical accuracy of CFD solution: Wavefront steepening along a tunnel

By inspection, the CFD solution reproduces the true behaviour quite well, especially in regions where the rates of change of pressure are approximately uniform, but errors begin to grow at the heel and toe of the wavefront, where large rates of change exist simultaneously in both space and time. This shows the existence of numerical diffusion in the CFD predictions and the consequences gradually extend outwards, both upstream and downstream. However, even in the extreme case where the wavefront is becoming a shock, the behaviour is reasonable, thus giving high confidence in the adequacy of the method of choosing the time-steps for the numerical integration process.

The *spatial* grid resolution is assessed in Fig-6, which shows solutions obtained independently with successively smaller grid sizes (varying by factors of 2) for a case with slots (width = 0.8 m) discussed below. Figure 6(a) shows predicted pressures at the point (x,y) = (245,0), namely at ground level 25 m outside the exit portal and Fig-6(b) shows mass flow rates through slots in the tunnel roof. The axial positions of the upstream ends of the slots are at x = 120 m, 150 m, 180 m and 210 m. The location of the chosen pressure history is consistent with many practical assessments of MPWs from real tunnels. The mass flow rates are not considered explicitly in practical design, partly because it would be too difficult to measure them and partly because they are not, in themselves, a significant cause of concern. They are a useful measure of the accuracy of the CFD methodology, however, because the velocity fields close to them exhibit strong spatial variations. Also, as discussed below (see Section 4), they may be regarded as an interface between the flow field inside and outside the tunnel. [NB: For the coarsest grid shown – i.e. Δx = 0.4 m – the grid local to the slots was reduced to 0.2 m so no curves are shown for mass flow through the slots].

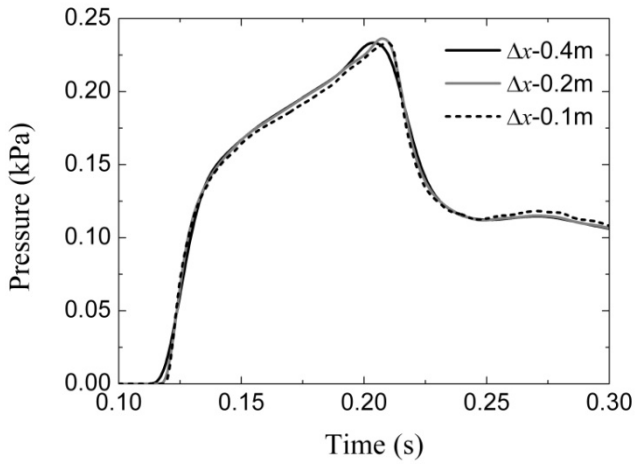

(a) $p\{t\}$ at (x,y) = (245,0)

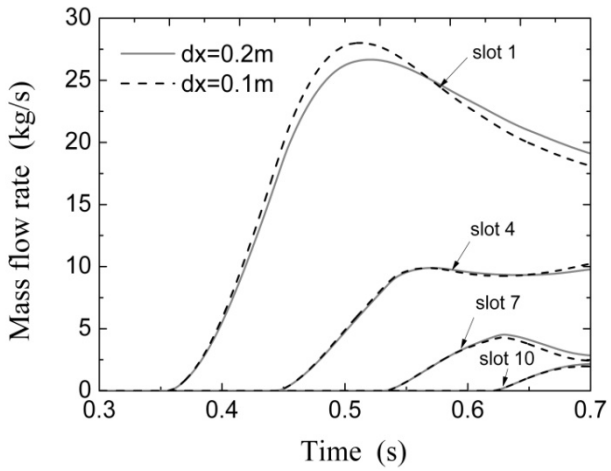

(b) Mass flow rates through slots 1, 4, 7 & 10

Fig-6 Assessment of numerical accuracy of CFD solution: Influence of spatial grid size ($\partial p/\partial t$ = 2 kPa in 0.1s)

It is considered that a grid size of 0.2 m would be adequate for the purposes of this paper, but all results presented below have nevertheless been obtained using a grid size of 0.1 m. As a consequence, it is reasonable to disregard the influence of numerical error and hence to regard the predictions as physically meaningful.

3 Exit region without slots

To provide a basis for comparisons, the analysis is applied first to a tunnel with no slots. Fig-7 shows successive pressure profiles along the floor of the tunnel (y = 0) as an incident pressure wave propagates towards the exit portal and afterwards. Before the instant when the toe of the wavefront reaches the portal plane, the waveform remains unchanged (except for steepening). After this instant, there is a strong reflection inside the tunnel and a weaker transmission outside it. The shape of the *reflected* wavefront is much less linear than the incident wavefront, but this is rarely of practical importance in tunnel design. In most 1-D analyses, the reflection is approximated as though each part of the incident wavefront reflected totally and instantaneously at the portal plane. If desired, however, it is possible to allow for the delays in a manner proposed by Rudinger [27] and used, for example, by Brown & Vardy [28]. Such delays cause a smoothed response that can be seen at the toe and heel of the reflected wavefront (which correspond respectively to the heel and toe of the incident wavefront).

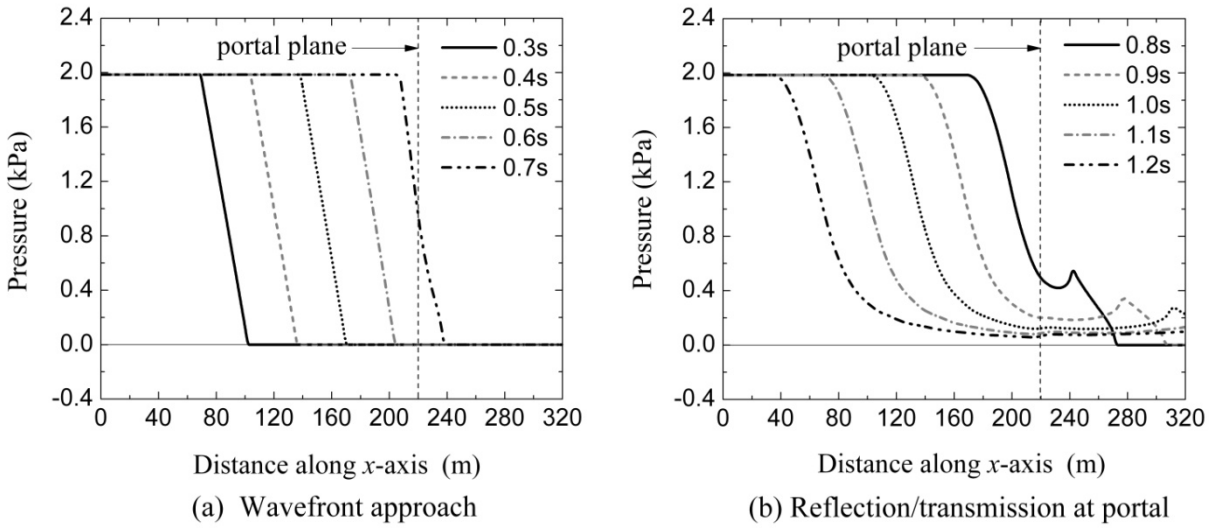

Fig-7 Pressure profiles along y=0. Unperforated exit (H_{tun}=8m)

Outside the tunnel, the wavefront initially behaves in the manner illustrated in Fig-2. Assuming that (as in this example) the wavefront ramp length exceeds the tunnel height, expansion waves from the roof of the tunnel will reach ground level (i.e. y = 0) before the incident pressure has reached its peak and so the maximum pressure experienced outside the tunnel at all $y \geq 0$ will be smaller than that of the incident wavefront. The longer the ramp, the greater the reduction and hence the smaller the amplitude of the transmitted MPW. Conversely, the greater the steepness of the incident wavefront the greater the amplitude of the MPW.

After the MPW has reached its peak, the pressure at the portal plane decreases as a consequence of the lateral expansion of the flow into the unbounded region outside the tunnel. Likewise, at

any location beyond the portal, soon after the initial pressure increase, a maximum is reached and the pressure then decays. In the case of a linear incident wavefront, the amplitude of this initial pulse is the main focus of MPW studies. With more general (non-linear) incident wavefronts, the peak MPW pressure will occur at a later time, but the underlying phenomenon is the same. Indeed, a good approximation to the non-linear behaviour can be obtained by regarding the wavefront as a succession of smaller, approximately linear wavefronts [29].

Fig-7 shows pressure distributions only along $y = 0$. However, the pressure disturbances *outside* the tunnel propagate in all directions - including the negative x-direction in the region above the tunnel, for instance. It would be impracticable to attempt to provide figures showing wave propagation throughout the simulation domain but important features of the behaviour can be inferred from graphs plotted along the reference line shown in Fig.8. The line is everywhere equidistant from the nearest point on the portal plane or the outer surface of the tunnel. The chosen distance, namely R =25m, is indicative of distances commonly used in full-scale and model-scale assessments of MPWs from tunnels.

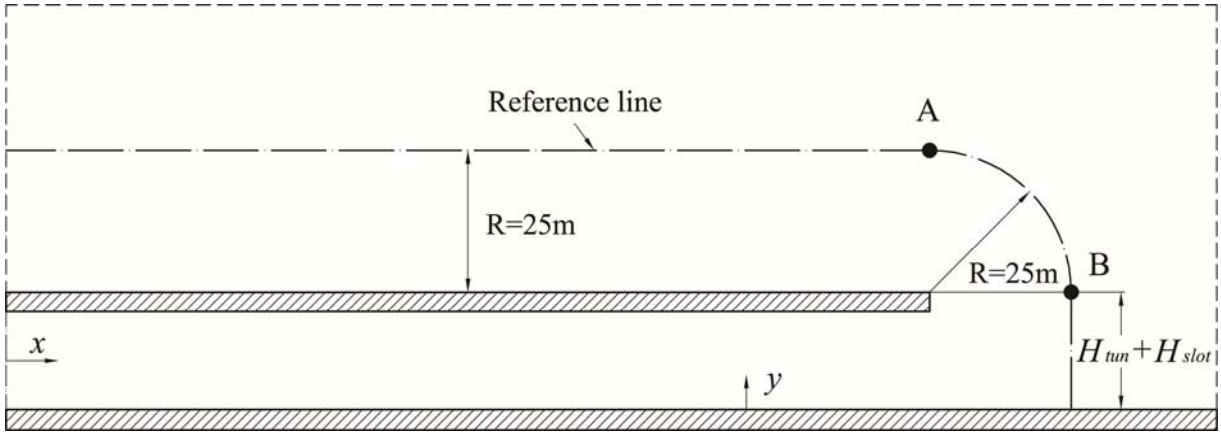

Fig-8 Reference line for MPW illustrations

Figure 9 shows successive pressure profiles along the reference line, the distance coordinate being measured along the line itself (i.e. not in a unique coordinate direction). Directly alongside the tunnel, the distance is equal to the axial coordinate x. This is followed by a distance $\frac{1}{2}\pi R$ along the circumference of an arc and then by a distance of $(H_{tun} + H_{roof})$ to the axis $y = 0$. The positions corresponding to the points A and B in Fig-8 are indicated by broken lines in the figure. Along the reference line, the pressure increases first at the locations closest to the portal. At later times, the pulse reaches successively greater distances along the line. At each instant, the greatest pressure is towards the leading part of the backward-propagating disturbance. However, the amplitude decreases with increasing time, i.e. with increasing distance from the portal. Similar behaviour exists along equivalent reference lines at other distances R from the tunnel, but with reduced amplitude as R increases.

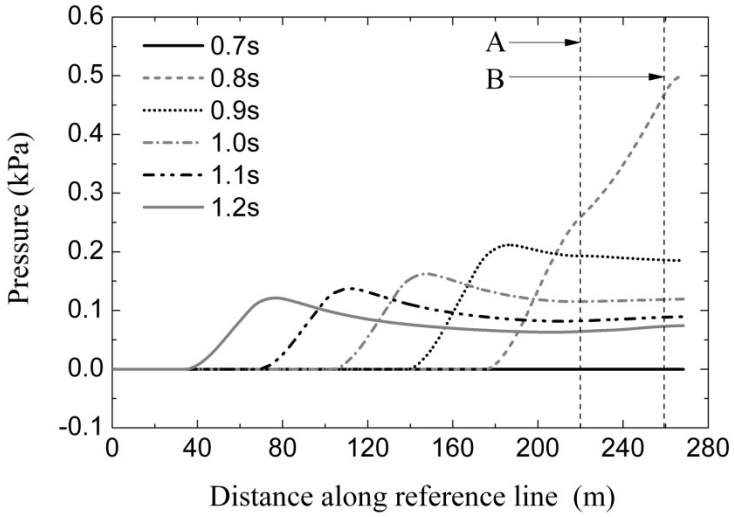

Fig-9 Pressure profiles along the reference line. Unperforated exit (H_{tun}=8m).
Note: Principal wave movement = right to left

4 Exit region with slots

The influence of roof slots is now considered. The chosen slotted region has an overall length of $12.5H_{tun}$ = 100 m and it has ten slots, each with a width of $W_{slot} = 0.1H_{tun}$ = 0.8 m, at regular intervals of $X_{slot} = 1.25H_{tun}$ = 10 m. The upstream edges of the first and last slots are at x = 120 m and x = 210 m, which is 10 m upstream of the portal plane. The thickness of the tunnel roof (and hence the height of the slots is $0.125H_{tun}$= 1 m. Successive pressure profiles along y = 0 are shown for this case in Fig-10 and they exhibit major differences from their counterparts in Fig-7. The *collective* influence of all of the slots is to cause a continual reduction in the amplitude of the wavefront as it propagates towards the exit portal. For the case shown, the residual amplitude at the exit is small. However, the leading part of the wavefront approaching the exit clearly exhibits the behaviour depicted in Fig-2(c). The effect is less strong than it would be if the incident wavefront were a sudden step, but it is nevertheless quite pronounced.

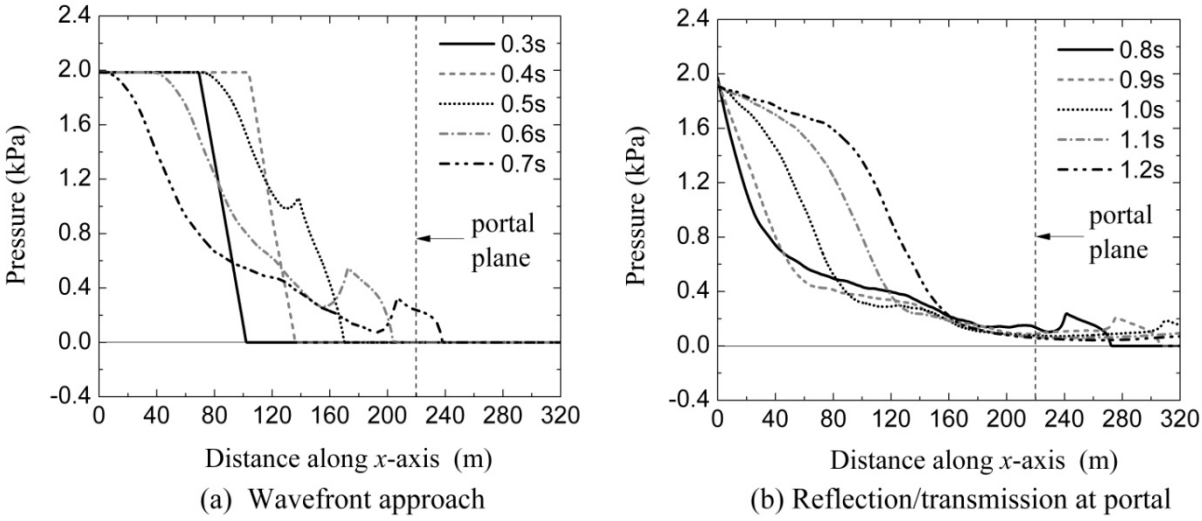

Fig-10 Pressure profiles along y=0. Perforated exit (H_{tun}=8m)

The predicted amplitude of the wavefront arriving at the portal plane is almost 80% smaller than in the case with no slots. However, the corresponding reduction in the amplitude of the MPW beyond the portal plane is less than 50%. There are two key reasons for this. First the amplitudes

of emitted MPWs are strongly dependent upon the *steepness* of incident wavefronts, much more so than on their amplitude; this is explored in more detail in Section 5. Second, the MPW amplitude is influenced by pressure disturbances emanating from the various slots as well as by the pressure disturbance from the main portal itself. This is because the disturbances from any particular slot propagate in all directions, including towards the exit portal. The influence of such flows can be inferred from Fig-11 which shows a sequence of pressure profiles along the reference line shown in Fig-8. Each profile may be regarded as a sum of contributions from several slots as well as from the main exit portal and so the outcome is more complex than that shown in Fig-9 for the case with no slots.

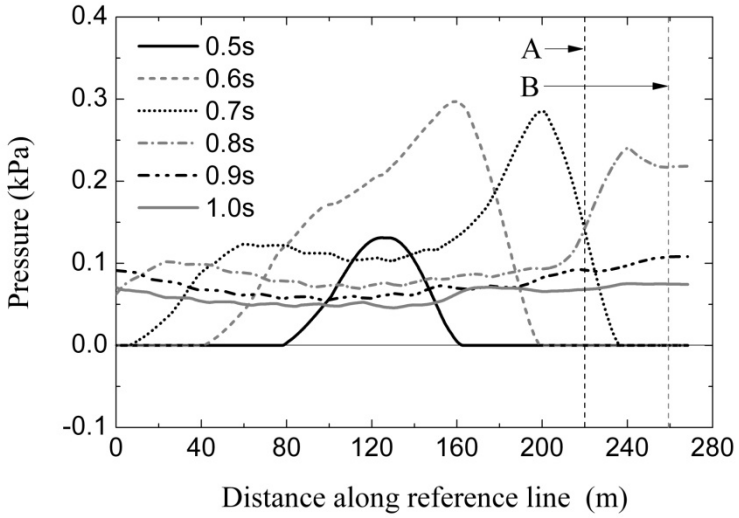

Fig-11 Pressure profiles along the reference line. Perforated exit (H_{tun}=8m).
Note: Principal direction of peak pressure = left to right

It can be seen from Fig-11 that the strong reduction in the amplitude of the incident wavefront at the exit has been achieved at the expense of allowing the development of significant pressures alongside the tunnel. This outcome is easily understood. If smaller slot widths were chosen, the predicted amplitudes of the lateral flows would reduce and so would the corresponding pressures alongside the tunnel. However, the beneficial influence of the slots on the internal wave propagation would reduce and so a lesser reduction in the MPW from the exit portal would result. The selection of optimum sizes and distributions of slots for any particular tunnel will depend upon the relative importance of the various locations outside the tunnel – e.g. the proximity of buildings or other locations that might be frequented by humans.

Fig-12 shows pressure histories at locations (a) on the reference line outside the tunnel and (b) at y = 0 inside the tunnel, at the axial locations of the 1st, 4th, 7th and 10th slots. By inspection, the strong reduction in amplitudes exhibited *inside* the tunnel is not reproduced *outside* the tunnel. Indeed, the maximum amplitudes alongside the 4th, 7th and 10th slots exceed that alongside the first slot even though the maximum rate of flow through the first slot exceeds that for any others. This outcome arises because of the superposition of waves. Specifically, pressures emanating from the 1st slot are experienced outside the subsequent slots simultaneously with pressures emanating from the individual slots themselves. The pressure history alongside the 1st slot is also a superposition of MPWs from all slots, but there is an important difference because *finite* superposition at that location cannot begin until after waves begin to arrive there from the second slot. In general, “upstream” superposition is much weaker than “downstream” superposition and the overall effect is of a downstream-moving phenomenon. [NB: Here, “downstream” is intended to imply the principal wavefront direction along the tunnel].

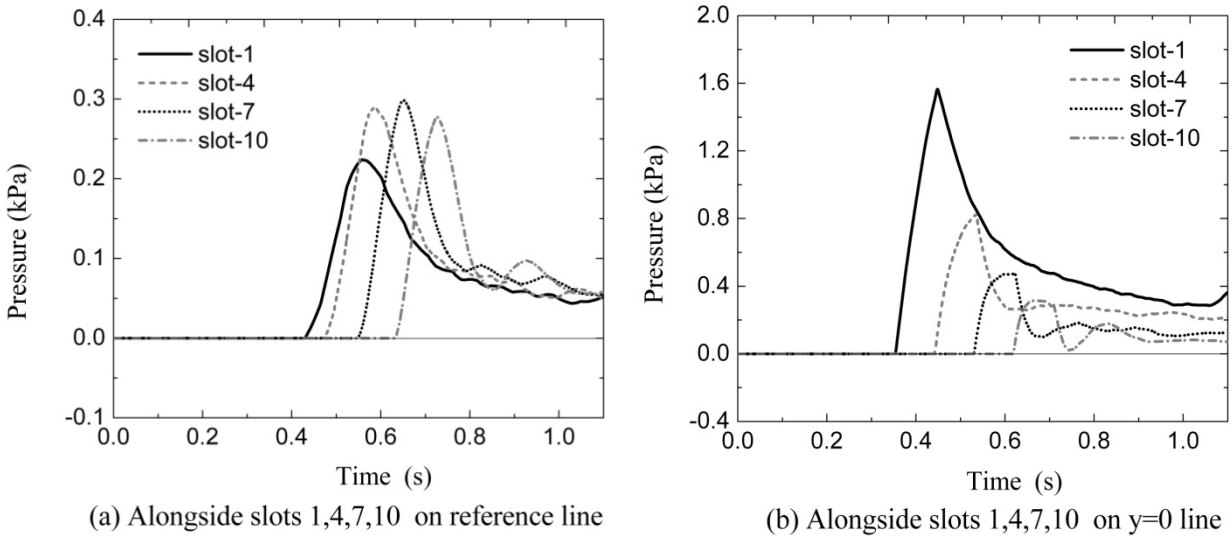

Fig-12 Pressure histories along the reference line and along $y = 0$, adjacent to slots 1, 4, 7 & 10 with upstream edges at x = 120 m, 150 m, 180 m & 210 m respectively
[*Note that different pressure scales are used in (a) & (b)*]

The mass flow rates through slots 1, 4, 7 & 10 for this case are presented above in Fig-6 (b) in Section 2.3, in which they have been discussed in relation to the assessment of numerical accuracy. For the purposes of the present section, however, attention focuses instead on physical and practical considerations. In many practical designs, the mass flow rates are used as an interface between independent solutions obtained for the regions of flow inside and outside a tunnel. Typically, the process begins with a 1-D numerical simulation of wave propagation inside the tunnel, based on an assumption of constant pressure at each outlet to the atmosphere. This is used to estimate rates of mass flow at the outlets and these are then used as input conditions for 3-D acoustic analyses outside the tunnel. The process is necessarily only approximate because the mass flows cause pressure variations at the outlets. However, the amplitudes of these variations are much smaller than those of the internal pressure waves so the simplification is acceptable for most practical purposes. Indeed, the errors arising from it will usually be smaller than errors inherent in the calculation of the internal pressure waves approaching the outlets. This is because 1-D analyses tend to be relatively poor at predicting rates of change of pressure even though they can be very good at predicting overall amplitudes of pressure waves. Furthermore, in the most commonly used methods of simulating the acoustic fields outside the tunnel, the tunnel outlets are approximated as point sources (equivalent to acoustic monopoles) in geometrically simple external domains. Also, when two or more outlets exist, it is usual to assume that their acoustic fields simply combine linearly. A big benefit of CFD analyses such as that presented herein is that the whole simulation of internal and external flows is undertaken simultaneously, thereby avoiding the need for any of these simplifications.

4.1 Reflected wavefront

Although the principal focus of this paper is on the potential influence of perforated extension regions on MPWs *outside* tunnels, the corresponding influence on wave propagation *inside* tunnels is also of practical importance (e.g. [17]). This will influence pressures experienced by passengers inside trains. Trains are the original cause of the incident wavefronts, but the main consequences for their passengers are not experienced until reflections of the waves arrive from downstream (e.g. from a portal or a perforated exit region). In engineering practice, wavefront propagation in long tunnels is almost always modelled using 1-D methods (because this is highly

cost-effective) so it is important to understand the degree to which the 2-D phenomena described above will influence the forms of reflected waves.

Figure 13 shows predicted pressure histories at (a) a representative location upstream of the first slot and (b) at successive locations along the perforated region. At each location, the 2-D prediction is compared with a corresponding prediction obtained using the 1-D software ThermoTun [30]. The latter has been developed for the specific purpose of simulating wave propagation in railway tunnels and it has been extensively validated for wave propagation in unperforated tunnels. Instead of modelling each slot discretely, the whole of the perforated region is treated as an homogeneous region with a total porous area equal to the sum of the areas of the ten slots.

It can be seen that the 1D methodology works well in the upstream region, but progressively less well further downstream. Only one comparison is shown upstream because comparisons at all other locations are almost identical. In the downstream region, however, the slots cause successive changes in the wave as it propagates and they also cause successive reflections, each of which is influenced by 2-D effects. In the early stages after the incident wavefront begins to arrive at the perforated region, only one slot exerts an influence. However, this is the most important slot because the incident wavefront is strongest at this location. At successive slots, the wavefront amplitude has already been reduced by upstream slots and any reflections from these downstream slots will be further reduced as they propagate back upstream. As a consequence, the early stages of the reflection process are more influential than the later stages.

In the upstream region, the dominant outcome is that the 1-D approximation works quite well and, as a consequence, it may be considered acceptable for practical design purposes, at least in principle. In the downstream region, the 1-D approximation works less well, but even in this region, it might be considered adequate for design purposes restricted to conditions *inside* the tunnel. This is because the errors are greatest where the pressure amplitudes are smallest. That is, although the proportional errors are relatively large, the absolute errors are not so large.

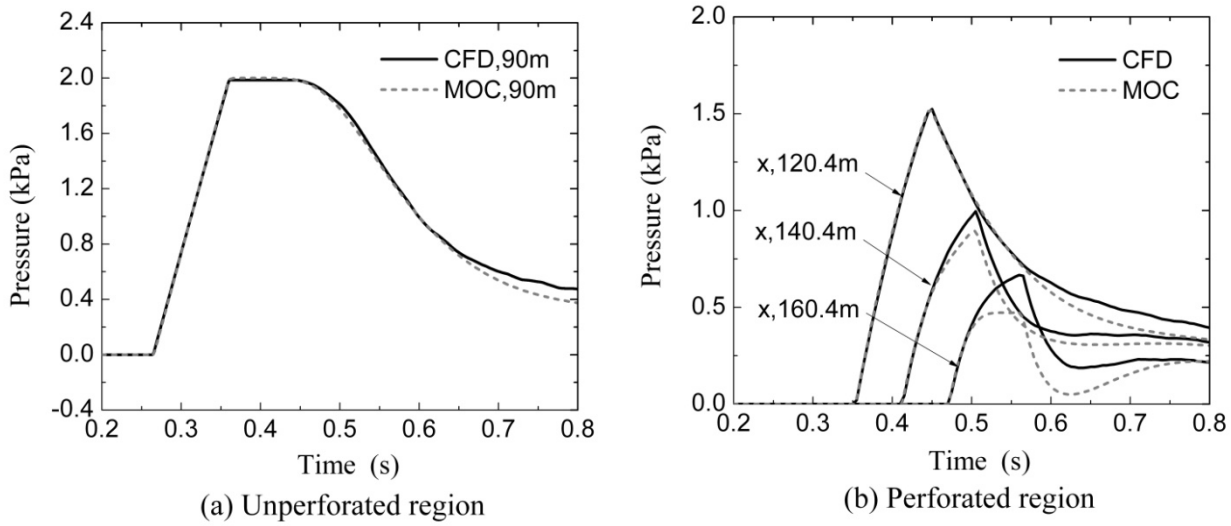

Fig-13 Influence of 2-D behaviour on wavefront propagation

Figure 13 illustrates what *can* be achieved with 1-D analysis, but it is not necessarily indicative of what *will* be achieved in any particular simulation. This is because 1-D outcomes are dependent on empirical judgement as well as upon mathematical rigour. Just as friction coefficients and local loss coefficients are empirical, so are parameters related to flows through slots. For Fig.13, the

assumed slot widths have been adjusted by a contraction coefficient of 0.6 and the assumed inertial lengths are 60% greater than the roof thickness - to allow for apparent mass effects. These values should not be regarded as optima, partly because few alternatives have been considered and partly because attention has focussed primarily on the reflected wavefront, in which the sensitivity to such parameters is relatively weak. A further limitation of 1-D methodology is that there is no practicable method of allowing directly for variations in atmospheric pressure just outside the slots. Such variations can be quite strong in timescales relevant to wave propagation – as evidenced, for example, by the principal focus of discussion in this paper.

5 Influence of wavefront steepness

All results presented above are for one particular incident wavefront. The amplitude of the chosen wave is broadly representative of likely combinations of the train:tunnel area ratio and the train speed. However, the steepnesses of such waves vary much more widely than their amplitudes, especially after the waves have propagated significant distances from their origins. Accordingly, it is useful to compare the outcomes presented above with corresponding outcomes for incident wavefronts of equal amplitude, but different steepnesses. Figure-14 shows pressure histories at three locations along the reference line for three rates of change of pressure, namely $0.5(\partial p/\partial t)_0$, $1.0(\partial p/\partial t)_0$ and $2.0(\partial p/\partial t)_0$, where $(\partial p/\partial t)_0$ =(2000/0.1)Pa/s is the indicative value used in the above examples. The chosen locations along the reference line are alongside slots 1 and 7 and on the axis $y = 0$. The upper and lower sets of boxes show predictions for the unperforated and perforated tunnels respectively. The time origins $t = 0$ used for the various graphs are synchronised with the leading toes of the incident wavefronts so the maximum pressures in the wavefronts are reached earlier with steep wavefronts than with less steep ones.

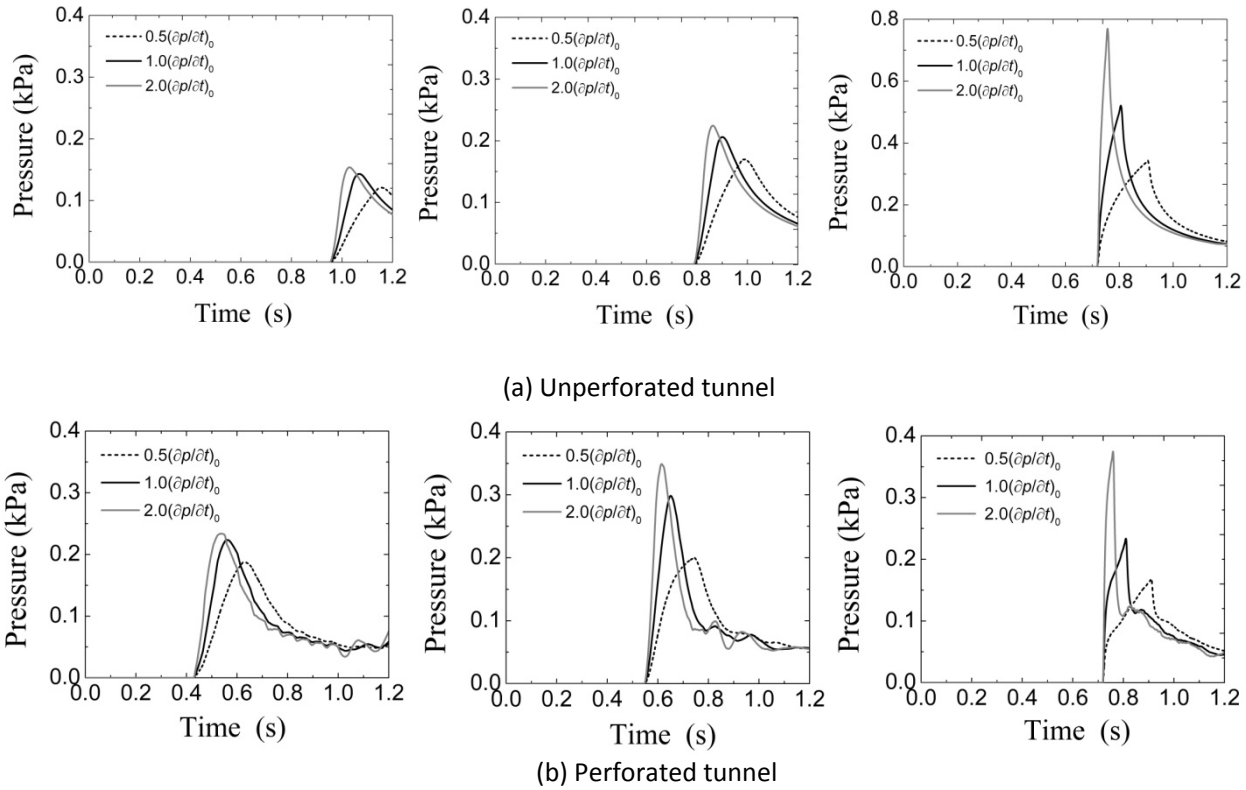

(a) Unperforated tunnel

(b) Perforated tunnel

Fig-14 Influence of incident wavefront steepness on MPWs along the reference line
(Left column: alongside slot-1 (x = 120.4m, y = 34 m),
Middle column: alongside slot-7 (x = 180.4m, y = 34 m),
Right column: at ground level, (x = 245m, y = 0 m);

Note different pressure scales used for perforated and unperforated tunnels)

For the unperforated exit region, the exit portal is the *only* source of the external disturbances. Therefore the MPWs occur first close to the portal and then spread upstream, influencing the slot-7 location before slot-1. In contrast, with the perforated region, the first MPW is emitted from the first slot and disturbance is experienced at slot-7 before $y = 0$ (beyond the portal). Maximum amplitudes of the MPWs in the regions alongside the tunnel and beyond the portal plane are listed in Table-3. For the unperforated tunnel, the same general trend is exhibited for each case. That is, the maximum MPW amplitude occurs beyond the portal and the amplitudes at successive locations decrease with increasing distance from the portal. For the perforated case, however, the location of the maximum MPW is not consistent in all cases. For the greatest steepness shown, the maximum MPW occurs beyond the portal. For successively smaller steepnesses, it occurs successively further from the portal. This has inconvenient consequences for practical design because it implies that the optimum slot areas will be dependent upon the steepness of the incident wavefront. This is a subject for more detailed consideration in future work.

At all locations, the predicted amplitude of the MPW increases strongly with increasing steepness of the incident wavefront even though the overall pressure amplitudes of the incident wavefronts are the same in all cases. This is the well-known result discussed above in relation to the mechanism depicted in Fig-2. However, the MPW amplitudes do not follow the widely reported trend of being approximately proportional to the steepness of the incident wavefront [6], even for the unperforated tunnel. This is a consequence of the two-dimensional nature of the geometrical domain depicted in Fig-2(b). Consider a wavefront expanding spherically in *three*-dimensional space from a point source. The overall surface area of the wavefront increases with the square of the radius and, as a consequence, the associated energy intensity decreases with the square of the radius and the pressure decreases linearly with the radius. If exactly analogous behaviour existed for a wavefront expanding cylindrically in two-dimensional space from a line source, the energy intensity would decrease with the radius and the pressure would decrease with the square root of the radius. Actually, this idealised analogous behaviour is not physically possible with the cylindrical geometry, but the values presented in Table-3 for the unperforated tunnel are nevertheless approximately consistent with this trend. The outcomes for the perforated tunnel are further influenced by the superposition effects discussed above and hence match the implied trend less closely. Nevertheless, for initial design purposes, a square-root dependence could be used as an approximate rule of thumb for the pressures beyond the portal.

Table-3 Maximum MPWs at locations along the reference line, kPa

Exit Region	**Steepness of incident wavefront** *NB:* $(\partial p/\partial t)_0 = 20$ *kPa/s*	**Maximum MPW alongside tunnel from (0,34) to (220,34)**		**Maximum MPW beyond portal plane from (220,34) to (245,0)**	
		Amplitude kPa	**Location (x), m**	**Amplitude kPa**	**Location (x,y), m**
Unperforated	$\frac{1}{2}(\partial p/\partial t)_0$	0.239	220	0.344	245, 0
	$(\partial p/\partial t)_0$	0.310	220	0.521	245, 0
	$2(\partial p/\partial t)_0$	0.356	220	0.770	245,0
Perforated	$\frac{1}{2}(\partial p/\partial t)_0$	0.217	152	0.168	245, 0
	$(\partial p/\partial t)_0$	0.300	172	0.282	220.5, 34
	$2(\partial p/\partial t)_0$	0.354	205	0.426	240.5, 23

For practical design, the effectiveness of perforated exit regions is likely to be quantified by the reduction achieved in MPW amplitudes. A simple, but common, generic way of doing this for other MPW counter-measures is by direct comparisons at a single point - typically a few diameters from the portal plane and subtending an angle of, say, 45° to the plane. Recently, site-specific comparisons have begun to receive increased attention, noting that the most sensitive locations are those where people are present (homes or workplaces, etc). Site-specific criteria also enable direct account to be taken of frequency distributions in emitted MPWs. For overview papers such as this, however, site-specific data are not available and, instead, the focus is on the generic performance. The most reasonable measure of effectiveness is the proportional reduction in the maximum MPW, wherever this might occur. Thus, for example, a major reduction close to the portal would be an inadequate guide if it were achieved only at the expense of strong MPWs elsewhere. Using this approach, the effectiveness of the illustrated region may be characterised using the ratio of the overall maximum MPWs listed in Table-3, irrespective of their location. Using this approach, the proportional reductions in MPW amplitude for the three wavefront steepnesses are

$\frac{1}{2}(\partial p/\partial t)_0$ (0.344-0.217)/0.344 = 37%
$(\partial p/\partial t)_0$ (0.521-0.300)/0.521 = 42%
$2(\partial p/\partial t)_0$ (0.770-0.426)/0.770 = 45%

These values may be compared with reductions of, typically, about 30% for other passive forms of MPW reduction cited in the introduction. It is noteworthy that the proportional effectiveness increases with increasing incident steepness. This will be a potentially valuable advantage in practical applications although, for the particular case of railway tunnel applications, all of the MPW amplitudes in Table-3 would be unacceptably large.

Regardless of the *proportional* effectiveness of the counter-measure, the practical target will usually be to achieve acceptable *absolute* amplitudes of the pressure disturbances. As a consequence, the engineering design challenge is critically sensitive to the reliability of estimating the steepness of the incident wavefront. This is inevitably a system-specific matter, dependent upon the design train speed and, usually to a lesser extent, on the train geometry. In the case of relatively short tunnels, the shape of the incident wavefront arriving at the exit region will be closely similar to that of the wavefront generated during nose-entry to the tunnel. This is because there is little time for the shape to evolve. In such cases, the incident wavefront can be predicted with reasonable accuracy provided that the train speed and the train geometry are known. With longer tunnels, additional uncertainties exist because strong changes can occur during wave propagation along a tunnel (steepening in the case of slab tracks, but perhaps elongation in the case of ballast tracks) and additional wave sources may exist (airshafts, etc). In all cases, however, although the ultimate suitability of the perforated exit region (or any other MPW counter-measure) cannot be assessed in isolation, the proportional reduction in MPW amplitudes is a useful measure of effectiveness.

6 Conclusions

The use of a long, perforated extension region to reduce the amplitudes of micro-pressure waves (MPWs) emitted from an open end of a duct has been investigated using a 2-D CFD analysis. The particular geometry studied is loosely representative of a railway tunnel emerging into a deep cut-and-cover region, but the overall flow behaviour has been interpreted in a manner that is equally applicable to many other applications. The principal conclusions may be summarised as follows:

1. The amplitudes of MPWs beyond exit portals can be reduced greatly by a perforated exit region, but this benefit is offset by increased amplitudes elsewhere – caused by disturbances emitted directly from the holes in the perforated roof.

2. The perforated region is more effective in reducing the *amplitudes* of incident waves reaching the exit portal than in reducing the maximum *steepnesses* thereof. This difference is important because MPW amplitudes depend more strongly on the latter than on the former.

3. The *proportional* reduction in MPW amplitudes achieved by a perforated exit region increases with increasing steepness of the incident wavefront. Nevertheless, the *absolute* amplitude of the emitted MPW increases with increasing wavefront steepness.

4. The performance of the perforated region is strongly influenced by 2-D characteristics of wave propagation. Strong pressure variations over the tunnel cross section arise because of the time required for waves from the slots to traverse the section. This effect is especially pronounced at the leading part of the main wavefront. This behaviour contrasts with that for unperforated regions – for which internal wavefront propagation approximates closely to plane wave behaviour until the wavefront reaches the tunnel portal.

5. The overall performance of a perforated exit region in reducing MPWs tends to be better than that of other passive methods of alleviation located in tunnel exit regions. Also, the provision of perforated regions for tunnels may be more acceptable visually than many other methods. Furthermore, in some cases, it might be possible to create them with only small modifications to the design of an unperforated portal region.

6. Strictly, all of these conclusions have been demonstrated only for planar 2-D geometry. This limits their direct applicability to small-times after waves reach the roof slots. The validity of the solutions decreases gradually as time increases.

Acknowledgements

The authors are grateful to the following bodies that provided financial support for the project: (i) China Scholarship Council, (ii) National Natural Science Foundation of China (Grant No. U1334201 and (iii) UK Engineering and Physical Sciences Research Council (Grant No. EP/G069441/1).

References

[1] Gawthorpe,RG (1978) Aerodynamics of trains in tunnels, *Railway Engineer International,* **3**(4), 41–47.

[2] Ravn,S & Reinke,P (2006) Tunnel aerodynamics of the magnetic levitation high-speed link in Munich(MAGLEV) – Consequences for pressure comfort, micro pressure waves, traction power and pressure loads, *Tunnel Management International Journal*, **9**(1),1-10.

[3] Montenegro,M & Vardy,AE (2013) Tunnel gradients and aural health criterion for train passengers, *Proc IMechE Part F: J Rail and Rapid Transit*, [***in press***].

[4] Vardy,AE & Hagenah,B (2006) Full-scale measurements in a tunnel airshaft, *Proc 9th int symp on Aerodynamics and Ventilation of Vehicle Tunnels, Portoroz, Slovenia, 11-13 July 2006*, BHR Group, 343-357.

[5] Gerbig,Ch & Degen,KG (2012) Acoustic assessment of micro-pressure wave emissions from high-speed railway tunnels, *Noise and Vibration Mitigation for Rail Transportation Systems, Notes on Numerical Fluid Mechanics and Multidisciplinary Design Volume*, **118**, 389-396.

[6] Ozawa,S, Maeda,T, Matsumura,T, Uchida,K, Kajiyama,H & Tanemoto,K (1991) Counter-measures to reduce micro-pressure waves radiating from exits of Shinkansen tunnels, *Proc 7th int symp on Aerodynamics and Ventilation of Vehicle Tunnels, Brighton, UK, 27-29 Nov 1991*, BHR Group, 253-266.

[7] Murray,PR & Howe,MS (2010) Influence of hood geometry on the compression wave generated by a high-speed train, *Journal of Sound and Vibration*, **329**(14), 2915–2927.

[8] Howe,MS, Iida,M & Fukuda,T (2003) Influence of an unvented tunnel entrance hood on the compression wave generated by a high-speed train, *Journal of Sound and Vibration*, **17(6)**, 833–853.

[9] Bellenoue,M, Auvity,B & Kageyama,T (2001) Blind hood effects on the compression wave generated by a train entering a tunnel, *Experimental Thermal and Fluid Science*, **25**, 397–407.

[10] Sockel,H & Pesave,P (2006) The reduction of micro pressure waves by baffles, *Proc 9th int symp on Aerodynamics and Ventilation of Vehicle Tunnels, Portoroz, Slovenia, 11-13 July 2006*, BHR Group, 804 – 817.

[11] Aoki,T, Vardy,AE & Brown,JMB (1999) Passive alleviation of micro-pressure waves from tunnel portals, *Journal of Sound and Vibration*, **220**(5), 921–940.

[12] Raghunathan,SR. Kim,HD & Setoguchi,T (2002) Aerodynamics of high-speed railway train, *Progress in Aerospace Sciences*, **38**, 469–514.

[13] Kim,H, Kweon,YH & Aoki,T (2004) A new technique for the control of a weak shock discharged from a tube, *Journal of Mechanical Engineering Science, Part C*, **218**(4), 377–387.

[14] Vardy,AE (2008) Generation and alleviation of sonic booms from rail tunnels, *Engineering & Computational Mechanics, Proc ICE*, **161**(EM3), 107-119.

[15] Matsubayashi,K, Kosaka,T & Kitamura,T (2004) Reduction of micro-pressure wave by active control of propagating compression wave in high speed tunnel, *Journal of Low Frequency Noise, Vibration and Active Control*, **23**(4), 259–270.

[16] Fukuda,T, Saito,S, Iida,M, Kurita,T & Ozawa,S (2013)] Countermeasure against the micro-pressure wave by a shelter linking neighboring tunnels, *Proc 15th int symp on Aerodynamics, Ventilation and Fire in Tunnels, Barcelona, Spain, 18-20 Sept 2013*, BHR Group, 539-552.

[17] Vardy,AE (1978) Reflections of step-wavefronts from perforated and flared tube extensions, *Journal of Sound and Vibration*, **59**(4), 577-589.

[18] Howe,MS & Cox,EA (2005) Reflection and transmission of a compression wave at a tunnel portal, *Journal of Fluids and Structures*, **20**, 1043-1056.

[19] Saito,S, Miyachi,T & Iida,M (2013) Countermeasure for Reducing Micro-pressure Wave Emitted from Railway Tunnel by Installing Hood at the Exit of Tunnel, *Quarterly Report of RTRI*, **54**(4), 231-236.

[20] Yang,YG, Zhu,K & Xi,BS (2001) One-Dimensional Simulation of the Pressure Wave near Exit of a High-Speed Train Tunnel, *Tsinghua Science and Technology*, **6**, 331-334.

[21] Baron,A, Mossi,M & Sibilla,S (2001) The alleviation of the aerodynamic drag and wave effects of high-speed trains in very long tunnels, *Journal of Wind Engineering and Industrial Aerodynamics*, **89**, 365-401.

[22] Mashimo,S, Nakatsu,E & Aoki,T (1997) Attenuation and Distortion of a Compression Wave Propagating in a High-Speed Railway Tunnel, *JSME International Journal, series B*, **40**(1), 51-57.

[23] Fukuda,T, Ozawa,S & Iida,M (2006) Distortion of Compression Wave Propagating through Very Long Tunnel with Slab Tracks, *JSME International Journal, series B*, **49**(4), 1156-1164.

[24] Miyachi,T, Fukuda,T & Iida,M (2008) Distortion of Compression Wave Propagating through Shinkansen Tunnel, Noise and Vibration Mitigation, *Notes on Numerical Fluid Mechanics*, **99**, 9-18.

[25] William-Louis,M & Tournier,C (2004) Numerical and experimental study of transversal pressure waves at a tube exit, *Experimental Thermal and Fluid Science*, **28**, 525-532.

[26] ANSYS FLUENT Manual, Release 14.0, 2011.

[27] Rudinger,G (1957) The reflection of pressure waves of finite amplitude from an open end of a duct, *Journal of Fluid Mechanics*, **3**(1), 48-66.

[28] Brown,JMB & Vardy,AE (1994) Reflections of pressure waves at tunnel portals, *Journal of Sound & Vibration*, **173**(1), 95-111.

[29] Matsuo,K, Aoki,T, Kashimura,H, Yasunobu,T and Mashimo,S (1994) Generation mechanism of impulsive wave emitted from high-speed tunnel exit, *Proc 8th int symp on Aerodynamics and Ventilation of Vehicle Tunnels, Liverpool, UK, 6-8 July 1994*, BHR Group, 199-209.

[30] *www.ThermoTun.com*.